Back Cover: Structural Biology of Cisplatin Complexes with Cellular Targets: The Adduct with Human Copper Chaperone Atox1 in Aqueous Solution (Chem. Eur. J. 37/2014)

ARTICLE *in* CHEMISTRY - A EUROPEAN JOURNAL · SEPTEMBER 2014

Impact Factor: 5.73 · DOI: 10.1002/chem.201402834

ChemPubSoc Europe

DOI: 10.1002/chem.201402834

CHEMISTRY A European Journal Full Paper

Computer Chemistry

Structural Biology of Cisplatin Complexes with Cellular Targets: The Adduct with Human Copper Chaperone Atox1 in Aqueous Solution

Vania Calandrini,[a, b] Trung Hai Nguyen,[a, b] Fabio Arnesano,[c] Angela Galliani,[c] Emiliano Ippoliti,[a, b] Paolo Carloni,*[a, b] and Giovanni Natile[c]

Abstract: Cisplatin is one of the most used anticancer drugs. Its cellular influx and delivery to target DNA may involve the copper chaperone Atox1 protein. Although the mode of binding is established by NMR spectroscopy measurements in solution—the Pt atom binds to Cys12 and Cys15 while retaining the two ammine groups—the structural determinants of the adduct are not known. Here a structural model by hybrid Car–Parrinello density functional theory-based QM/MM simulations is provided. The platinated site minimally modifies the fold of the protein. The calculated NMR and CD spectral properties are fully consistent with the experimental data. Our in silico/in vitro approach provides, together with previous studies, an unprecedented view into the structural biology of cisplatin–protein adducts.

Introduction

Cisplatin (*cis*-diamminedichloridoplatinum(II)) is one of the most widely used drugs in anticancer chemotherapy.[1–6] Its antitumor activity is due to the formation of stable adducts with DNA.[7,8] Unfortunately, after repeated administrations of the drug, cancer cells develop resistance mechanisms, which strongly limit cisplatin efficacy.[1,3,4] The decreased accumulation of cisplatin by a decreased uptake and by an increased drug efflux and sequestration is among the proposed mechanisms leading to resistance.[3,4,9] Cisplatin may enter the cell via human copper transport proteins,[4,10–14] including the high-affinity copper transporter Ctr1;[15] while the ATPase copper pumps ATP7A/ATP7B could be responsible for sequestration and efflux of cisplatin;[16,17] finally, the copper chaperone Atox1 could deliver platinum (Pt) to the ATPases[18,19] and also be involved in the influx of cisplatin by controlling the cisplatin-induced down regulation of Ctr1 through ubiquitination.[10,20] Moreover, Atox1 has been found to translocate to the nucleus in response to copper exposure,[21] which raises the question of whether it could also be involved in the delivery of cisplatin to DNA.

Designing new Pt-based compounds able to reduce drug resistance problems related to their access to tumor cells requires an understanding of the Pt coordination chemistry to the proteins involved in resistance. Recently, using a combination of QM/MM and computational spectroscopy approaches, along with experimental data, we have characterized the binding modes of cisplatin to one of the extracellular methionine-rich motifs of yeast Ctr1 (Met7) in aqueous solution.[22] This study suggested that the platinated peptide $[PtX]^+$-(M*TGM*KGM*S), with X = Cl^- or OH^-, is the most relevant species occurring in solution. An investigation of cisplatin binding to the first N-terminal copper binding motif of the human ATP7A in aqueous solution (Mnk1) led to the conclusion that, differently from Met7, the Pt substrate keeps the two *cis* ammines and coordinates to the sulfur atoms of Cys19 and Cys22 of the highly conserved CxxC sequence.[23,24] So far, cisplatin binding to Atox1 in water solution has been inferred from electrospray ionization mass spectrometry (ESI MS) and nuclear magnetic resonance (NMR) spectroscopy.[25,26] These data show that, similarly to what happens in the reaction with the structurally similar Mnk1, in solution the $[Pt(NH_3)_2]^{2+}$ moiety binds to Cys12 and Cy15 residues of Atox1 keeping the two ammines and that the adduct is monomeric[25,26] (Scheme 1). Note that this binding mode is different from the one evidenced in crystallographic structures,[27] where 1:1 and 1:2 complexes between human Atox1 and cisplatin have been observed with different coordination to that in solution.[27] In two recent reports it has been unambiguously shown that Cu^I promotes the

[a] Dr. V. Calandrini, Dr. T. H. Nguyen, Dr. E. Ippoliti, Prof. Dr. P. Carloni
Computational Biophysics
German Research School for Simulation Sciences
52425 Jülich (Germany)
and
Computational Biomedicine
Institute for Advanced Simulation IAS-5
Forschungszentrum Jülich, 52425 (Germany)

[b] Dr. V. Calandrini, Dr. T. H. Nguyen, Dr. E. Ippoliti, Prof. Dr. P. Carloni
Computational Biomedicine, Institute of Neuroscience and Medicine INM-9
Forschungszentrum Jülich, 52425 Jülich (Germany)
E-mail: p.carloni@grs-sim.de

[c] Dr. F. Arnesano, Dr. A. Galliani, Prof. G. Natile
Department of Chemistry, University of Bari "A. Moro"
via Edoardo Orabona 4, 70125 Bari (Italy)

Supporting information for this article is available on the WWW under http://dx.doi.org/10.1002/chem.201402834.

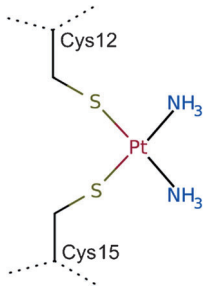

Scheme 1. Binding mode of cisplatin to Atox1 in aqueous solution, emerging from ESI-MS and $^{1}H,^{13}C$ and $^{1}H,^{15}N$ HSQC measurements.

platination of Atox1 at the CxxC Cu^{I}-binding site.[19,23] They showed that one equivalent of cisplatin added to apo Atox1 causes little, if any, protein unfolding over two weeks, while addition of one equivalent of cisplatin to Cu^{I}–Atox1 results in unfolding and aggregation with a half-life of about two days.[19,23]

As a further step in the characterization of the interaction of cisplatin with Atox1, here we provide the first 3D structure of an overall model adduct consistent with all the experimental data of the platinated complex in solution. Specifically, we performed molecular simulation-based structural prediction of the complex, based on the binding mode in Scheme 1. The consistency of the predicted 3D Pt coordination is tested against previously published[25] and new experimental spectroscopic data. Since electronic structure effects are important for the stereochemistry of transition metal ions, we use hybrid Car–Parrinello density functional theory-based (DFT) QM/MM simulations. The platinated site is treated within the density functional approach, whilst the rest of the system is treated with classical all-atom force fields (the Amber parm99[28] with the "Stony Brook" modification[29] for the peptide, and the TIP3P[30] for the water molecules). The predicted model has ^{1}H, ^{13}C, and ^{15}N NMR chemical shifts and circular dichroism (CD) spectra in accord with the experimental data, providing, for the first time, a reliable structural model of the adduct between Atox1 and cisplatin in solution.

Results and Discussion

The structural models of apo Atox1 and its Pt-adduct in aqueous solution, as they emerge from our QM/MM simulations, are reported in Figure 1. Comparison is made with CD spectra reported in reference [25] as well as with NMR spectroscopy data measured here.

Global fold

Apo Atox1

The QM/MM-averaged RMSDs of the backbone is 1.63(±0.03) Å, as compared with 0.8(±0.1) Å from the experimental NMR structure.[31] The number of NOE restraint violations is comparable to that of the NMR structure.[31] All these findings indicate that there is a good agreement between the structure of apo Atox1, as it emerges from our QM/MM simulations, and that determined by NMR spectroscopy.

The average number of residues involved in helical structures predicted by QM/MM compares fairly well with the experimental structure (Table 1, and Figure S2 in the Supporting Information). Standard deviations are reported in parentheses in Table 1.

Table 1. Average number of residues involved in secondary structures calculated[a] by DSSP.[32,33]

	Apo Atox1 from NMR structure[31]	Apo Atox1 from this QM/MM simulation	Pt-adduct from this QM/MM simulation
no. residues in helices	23 (1)	19 (2)	19 (3)
no. residues in β-sheets	20 (2)	22 (1)	22 (1)

[a] For the simulated systems (apo Atox1 and Pt-adduct) the analysis has been performed over 100 snapshots taken through the QM/MM trajectories, while for the experimental counter part of apo Atox1 we used the NMR structure.[31] The numbers in parentheses are standard deviations.

As for the number of residues involved in H bonds, the average number in the apo model is 52±1, to be compared with 52±2 obtained for the experimental NMR structure[31] (Table 2) A detailed view of the H bonds formed in both the main chain and the side chains of our models is given in Tables S13 and S14 in the Supporting Information.

The calculated CD spectrum is in good agreement with the experimental one (Figure 2). Both calculated and experimental spectra show a positive band at approximately 195 nm and a negative band at about 210 nm.

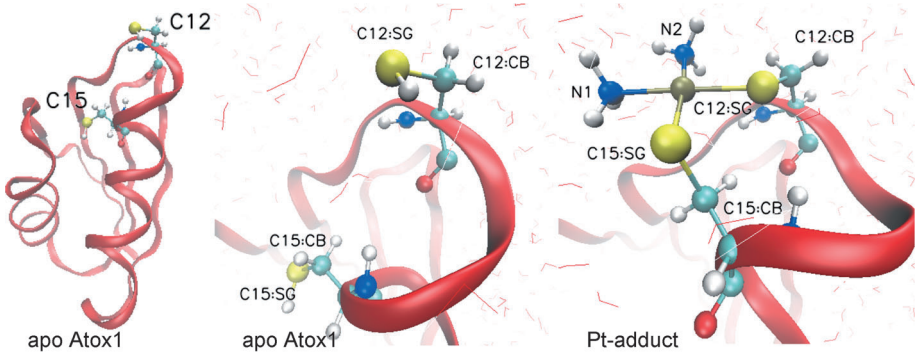

Figure 1. Structural models of apo Atox1 and its Pt-adduct in aqueous solution as they emerge from QM/MM simulations (left: Atox1 backbone along with Cys12 and Cys15 side chains; center: close up on the Cys12/Cys15 region in apo Atox1; right: close up on the Cys12/Cys15 region in the Pt-adduct). The backbone of the protein is represented by a red ribbon. Cys12 and Cys15 residues, along with the Pt moiety, are represented in balls and sticks with the following color code: platinum in brown, sulfur in yellow, carbon in cyan, nitrogen in blue, and hydrogen in white. Water molecules are represented by lines in which the oxygen is colored in red, and the hydrogen in white.

Pt-adduct

The coordination of the $[Pt(NH_3)_2]^{2+}$ moiety to Atox1, as shown in Scheme 1, turns out to

Table 2. Average number of residues with H-bonds calculated[a] by VADAR.[34]

	apo Atox1 from NMR structure[31]	apo Atox1 from this QM/MM simulation	Pt-adduct from this QM/MM simulation
no. residues with H bonds	52 (2)	52 (1)	53 (2)

[a] For the simulated systems (apo Atox1 and Pt-adduct) the analysis has been performed over 15 snapshots taken through the QM/MM trajectories, while for the experimental counter part of apo Atox1 we used the NMR structure.[31] The numbers in parentheses are the standard deviations.

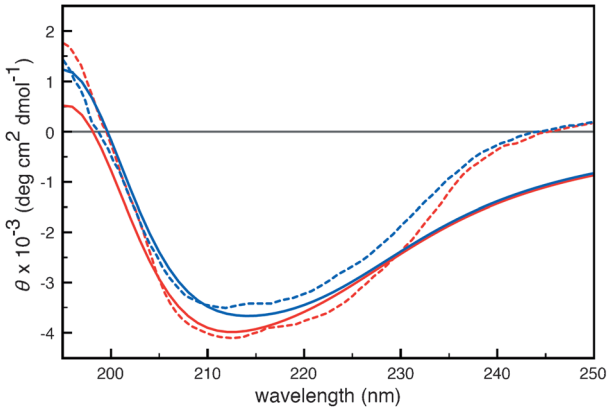

Figure 2. Calculated (continuous lines) and experimental[24] (dashed lines) CD spectra of apo Atox1 (red) and its Pt-adduct (blue). The calculated CD were obtained by averaging 100 snapshots of the QM/MM trajectories over the last 10 ps.

only marginally affect the overall conformation of the protein. It is simply achieved by rotating the side arms of the two binding cysteines (Figure 1). Whilst the β-sheets of the two models are very similar, the first α-helix, close to the binding site, turns out to be partly destabilized. This decrease in α-helix content is compensated by an increase of the 3_{10}-helices, located between the second and the third β-strand, and at the end of the second α-helix (Figure S2 in the Supporting Information). We conclude that the helical and β-sheet content remain essentially constant upon platination (Table 1). This finding is also confirmed by the fact that, in general, the evolution of the torsion angles ϕ and ψ along the protein backbone do not qualitatively change upon platination (Tables S8 and S9, and Figure S3 in the Supporting Information), thus indicating that the typical secondary structure elements are essentially conserved. The small variations of ψ, usually associated to a transition from α-helix to 3_{10}-helix, are within our error bars. Also, the ω angle remains very close to a planar geometry, thus indicating that no distortions are induced in the backbone (see Table S10 and Figure S3 in the Supporting Information). Consistently, both experimental and calculated CD spectra show that platination does not lead to any substantial shift of the positive and negative bands observed for apo Atox1. The main feature of the experimentally determined spectra was a reduction in intensity of the negative band upon platination. Such a change is reproduced also by the computed spectra (Figure 2). In addition we note that the average number of residues involved in H bonds (Table 2) as well as the number of H bonds formed in the main chain (Table S13 in the Supporting Information) remain essentially constant upon platination, which is a further indication that the global fold of the protein does not change upon cisplatin binding. The number of H bonds formed in the side chains is instead higher in the Pt-adduct than in the apo protein, (23 vs. 13, see Table S14 in the Supporting Information). A detailed description of the H bonds formed in both the main chain and the side chains of our models is given in Tables S13 and S14 in the Supporting Information. The agreement between calculated and experimental CD data supports the reliability of our model in describing platination of Atox1 in solution. The quality of the model is further supported by its Ramachandran plot (Figure S4 in the Supporting Information).

Pt-coordination geometry

The Pt-coordination geometry is close to an ideal square-plane (see Figure 1 and Table S7 in the Supporting Information; maximum deviation from the mean plane of the donor atoms of 0.07 Å for Pt atom with a standard deviation of 0.05 Å). The Pt–N distances are 2.14(5) and 2.13(5) Å. The Pt–S distances are 2.37(5) and 2.37(5) Å. This may be compared with the values of 1.99 and 1.80 Å for Pt–N and 2.31 and 2.10 Å for Pt–S bonds in the X-ray structure of the Atox1 dimer (resolution 2.14 Å) where the metal ion of $[Pt(NH_3)_2]^{2+}$ bridges Cys15 (chain A) and Cys15 (chain B) in *cis* position.[27]

The N-Pt-N and S-Pt-S angles are 88(3)° and 89(4)°, respectively. The S-Pt-S angle is very close to the theoretical value of 90° and much smaller than that found in the $[Pt(NH_3)_2]^{2+}$–$(Atox1)_2$ dimer which was as large as 111°.[27] This suggests that, because of flexibility of cysteine side chains, there is no strain in the large chelate ring of the $[Pt(NH_3)_2]^{2+}$–Atox1 monomer. That the cysteine side chains allow for significant flexibility in chelate-ring formation is also witnessed by the *trans* (as opposed to *cis*) arrangement of the sulfur atoms in the Pt(Atox1)(TCEP) monomer reported by Rosenzweig et al.[27] The N-Pt-S angles are 95(3)° and 88(3)°.

As a last point we note that two hydrogen bonds involving the main chain and the side chains of residues in the Pt binding site are lost upon cisplatin coordination (Tables S13 and S14 in the Supporting Information).

Comparison between experimental and computational NMR data of the platinated site

In order to avoid interference from reducing agents (usually employed in investigations with easily oxidizable proteins such as Atox1), we performed an NMR experiment on a fully ^{15}N-labeled and selectively ^{13}C-cysteine-labeled Atox1 (^{15}N,^{13}C-Cys Atox1 hereafter), in 50 mM phosphate buffer (pH 7.0) at 25 °C under inert N_2 atmosphere, in the absence of any reducing agent. ^{15}N-labeled cisplatin was added to the protein solution

(100 μM) to obtain an equimolar mixture and the reaction was monitored through $^{1}H,^{13}C$ and $^{1}H,^{15}N$ HSQC spectra.

The 2D $^{1}H,^{13}C$ HSQC spectra of $^{15}N,^{13}C$-Cys Atox1 in the absence (blue contours) and in the presence (red contours) of one equivalent of cisplatin (48 h after mixing) are shown in Figure 3. It can be noted that only β-methylene groups of Cys12 and Cys15 undergo change of chemical shift upon platinum coordination, while Cys41 signals are not affected.

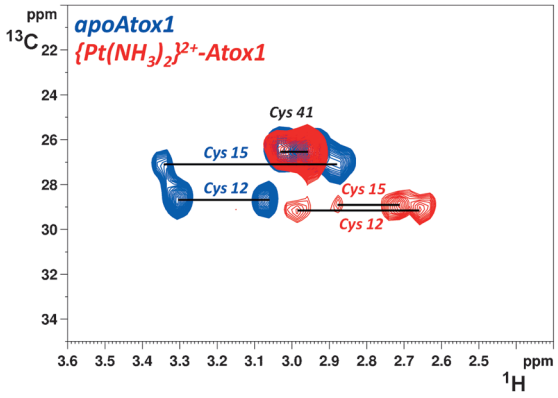

Figure 3. Overlay of 2D $^{1}H,^{13}C$ HSQC spectra of $^{15}N,^{13}C$-Cys Atox1 in the absence (blue contours) and in the presence (red contours) of one equivalent of cisplatin (48 h after mixing). The assignment of cysteine β-methylene groups for apo Atox1 and the cisplatin adduct is shown.

In Figure 4 are shown the 2D $^{1}H,^{15}N$ HSQC spectra of *cis*-$[PtCl_2(^{15}NH_3)_2]$ treated at pH 7.0 with one equivalent of apo Atox1 soon after mixing (blue contours) and after 48 h of incubation (red contours). Initially, only cross-peaks characteristic of $^{15}NH_3$ *trans* to O or Cl are observed; in contrast, after 48 h, only cross-peaks characteristic of $^{15}NH_3$ *trans* to S donor atoms, are visible.

Our calculated ^{1}H and ^{13}C chemical shifts of the β-methylene groups of Cys12 and Cys15 side chains (Table 3) reproduce the experimental data within one standard deviation (reported in parentheses in Table 3), or, in the worst cases, within the typical error due to the employed level of theory (7.6 ppm for ^{13}C chemical shift[35] and 0.5–1 ppm for ^{1}H chemical shifts[36]) for both apo and Pt–Atox1. Note that since the experiment does not allow the specific assignment of the chemical shifts to the $H_{\beta 2}$ and $H_{\beta 3}$ nuclei, the comparison for ^{1}H chemical shifts is made between the averaged values with standard deviation computed from error propagation. In addition, our calculations predict for the Cβ carbon of Cys12 and Cys15 a small downfield shift upon platination (Table 3), which is compatible with the downfield shift observed experimentally (Table 3 and Figure 3).

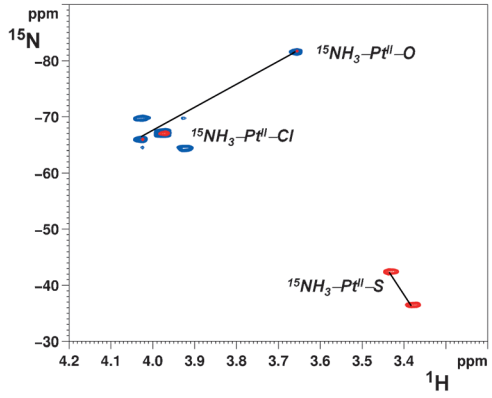

Figure 4. 2D $^{1}H,^{15}N$ HSQC spectra of *cis*-$[PtCl_2(^{15}NH_3)_2]$ treated at pH 7.0 with one equivalent of apo Atox1 soon after mixing (blue contours) and after 48 h of incubation (red contours). Cross-peaks are assigned to $^{15}NH_3$ *trans* to O, Cl, or S donor atoms, respectively. Cross-peaks belonging to the same species are connected by a straight line.

Table 3. ^{13}C (top) and ^{1}H (bottom) NMR chemical shifts (in ppm) of apo Atox1 and its Pt-adduct.[a]

Residue	Atom name	Apo Atox1 simulation	Pt-adduct simulation		Apo Atox1 experiment	Pt-adduct experiment
Cys12	C_β	31.7 (3.9)	35.7 (4.0)		28.7	29.1
Cys15	C_β	29.4 (3.7)	35.9 (4.0)		27.1	28.9
Residue	Atom name	Apo Atox1 simulation	Pt-adduct simulation	Atom name	Apo Atox1 experiment	Pt-adduct experiment
Cys12	$H_\beta 2$	3.9 (0.5)	3.8 (0.5)	H_β*	3.31, 3.06	2.99, 2.66
	$H_\beta 3$	3.3 (0.5)	3.4 (0.6)			
Cys15	$H_\beta 2$	3.8 (0.6)	3.4 (0.5)	H_β*	3.34, 2.87	2.88, 2.71
	$H_\beta 3$	2.6 (0.4)	3.4 (0.6)			

[a] The numbers reported in parentheses are the standard deviations. Note that the experimental values of the chemical shifts of $H_{\beta 2}$ and $H_{\beta 3}$ nuclei are generically indicated as H_β* since the stereospecific assignment is lacking.

We next compare the experimental and calculated ^{15}N and ^{1}H chemical shifts of the Pt-bound ammine ligands. The ^{15}N chemical shift is very sensitive to the nature of the donor atom in the *trans* position, and therefore may be very diagnostic of the presence of sulfur coordination.[37,38] Note that since the experiment does not allow the ^{15}N chemical shifts to be univocally assigned to the amine ligands *trans* to Cys12 or to Cys15, the differences between theoretical and experimental data are estimated using the average values. The calculated ^{15}N chemical shifts, averaged over the two ammine nitrogen atoms, deviate from the experimental values by approximately 9 ppm, which is above one standard deviation of the mean (~6 ppm), but still well below the typical error associated to this level of theory (13–16 ppm;[39] Table 4). These theoretical data thus correctly reproduce one of the most important experimental findings in favor of the presence of $^{15}NH_3$ groups *trans* to the S atoms of Cys12 and Cys15.

Also, in the case of the chemical shifts of the amminic protons, the differences between theoretical and experimental data are estimated using the average values. The calculated values are consistent with the experimental ones within one standard deviation, or, in the worst cases, within the mean error intrinsic to the employed level of theory (0.5–1 ppm).[36]

We, therefore, conclude that the predicted model, the spectroscopic data of which are in accord with the solution NMR

Table 4. ^{15}N (top) and ^{1}H (bottom) NMR chemical shifts (in ppm) of the ammine ligands in cisplatin and in Atox1-cisplatin adduct.[a]

Atom name	Cisplatin simulation	Pt-adduct simulation	Atom name	Cisplatin experiment	Pt-adduct experiment
N1	reference	−44.1 (7.8)	N*	−67.1, −67.1	−42.5, −36.5
N2	reference	−52.1 (8.1)			
HN1	3.9 (0.3)	3.8 (0.1)	H*	3.97, 3.97	3.43, 3.38
HN2	3.9 (0.3)	4.1 (0.2)			

[a] The numbers reported in parentheses are the standard deviations. Note that cisplatin (*cis*-[$PtCl_2(^{15}NH_3)_2$]) is used as a secondary reference in the theoretical calculations. The experimental values of the chemical shifts of ^{15}N and ^{1}H nuclei of amine groups are generically indicated as N* and H*, respectively, since the stereospecific assignment is lacking.

and CD data, represents a reliable structural model for the adduct of Atox1 with cisplatin.

Conclusion

Our calculations allow the prediction of the 3D structure of the Atox1–cisplatin chelate adduct in solution. The Pt-binding mode turns out to be rather similar to that of the first domain of ATP7A, Mnk1.[23,24] The model is fully consistent with the available spectroscopic data in solution from reference [25] and measured here. This work, along with our previous investigations,[22,24] provides a first semiquantitative look at the Pt stereochemistry in adducts of cisplatin with known cellular targets (see Table S7 in the Supporting Information for structural parameters of Atox1–cisplatin chelate adduct). The model is freely available in the Supporting Information.

Computational Methods

QM/MM calculations

For apo Atox1 we used the monomeric structure solved by NMR spectroscopy.[31] The Pt-moiety, $Pt(NH_3)_2^{+2}$, was docked onto the C12xxC15 motif of the apo form of Atox1 assuming the binding mode suggested by solution NMR spectroscopy[24] with standard bond lengths and angles (see the Supporting Information). Both apo Atox1 and Pt-adduct were solvated in a water box of about $7\times7\times7$ nm^3. The systems contained about 33000 atoms. No counterions were added, as the systems were neutral. The two systems were subjected to 0.2 μs of preparatory classical molecular dynamics simulations in order to provide initial structural models for the hybrid Car–Parrinello QM/MM simulations.[40–44] For the Pt moiety of the Pt-adduct we used an approximate force field and for the protein the AMBER force field (see the Supporting Information for more details). The structures for the QM/MM simulations were selected by a cluster analysis[45] over the last 0.2 μs of the converged MD trajectories (Figure S1 in the Supporting Information). Only one cluster was sufficient to represent about 80% of the conformational space explored by each system during MD simulations. QM/MM simulations were carried out using the CPMD program combined with the classical MD GROMOS96 code,[46] through the interface developed by Rothlisberger's group.[44] Each system was divided in two parts, a QM part and a MM part. The first part includes the atoms of the protein chain located between the C atom of Thr11 and the Cα atom of Ala16, along with the platinated moieties in the case of the Pt-adduct. This part was treated by DFT, with the functional BLYP for the exchange and correlation energies.[47,48] The wave function was expanded in a plane-wave basis set up to an energy cutoff of 90 Ry. Only the valence electrons were treated explicitly (in the case of Pt, electrons in the $n=5$ shell are also included in the valence), while the core electrons were described using norm-conserving pseudopotentials of the Martins–Troullier type.[49] The dangling bonds in between the QM and MM regions[50] were saturated using an adapted monovalent carbon pseudopotential. Isolated system conditions were imposed in the QM part by employing the Martyna–Tuckerman scheme.[51] The MM part includes the rest of the system (part of the protein and the solvent) and is described by the same force fields employed in the classical MD simulations. The electrostatic coupling between the QM and MM part were calculated using a fully Hamiltonian hierarchical approach.[44] In particular, the interactions were explicitly computed for all classical atoms within a distance of 5.3 Å from any QM atom using a modified Coulomb potential to prevent electron spill-out.[44] For distances between 5.3 and 10.6 Å, the interactions were calculated using the D-RESP charge scheme,[43] while above a distance of 10.6 Å a multipole expansion scheme was employed.[44] A fictitious electronic mass of 500 a.u. and a time step of 0.097 fs were used for the Car–Parrinello dynamics. Constant temperature conditions were achieved using the Nose–Hoover chain thermostat.[52–54] The 5000 steps of annealing were performed to relax the selected structures from the previous MD simulations. Then, the systems were heated up to 300 K by increasing the temperature with a rate of approximately 20 K every 1000 steps. Finally, 15 ps long QM/MM simulations were carried out.

Computational spectroscopy

^{1}H and ^{13}C NMR chemical shielding constants were calculated as averages over 100 equidistant snapshots extracted from the last 10 ps of the QM/MM trajectories. To maintain coherently the same level of theory used for the dynamics, these calculations were carried out by employing the approach of references [55,56], which is based on the BLYP gradient corrected functional combined with a pseudopotential plane wave representation of the electronic structure in the frozen core approximation (in our case the norm-conserving pseudopotentials of the Martins–Troullier type). This level of theory provides very good estimation for the ^{1}H shifts (the typical error with respect to the experimental values ranges between 0.5–1.0 ppm),[36] while for ^{13}C is less satisfactory but still good.[56] Indeed, it has been shown that the core electrons' contribution to the chemical shifts is almost constant,[57] and using as a reference a compound with similar coordination, the error essentially cancels out. As for the error due to the use of the BLYP functional, it has been estimated to be of the order of approximately 7.6 ppm for ^{13}C.[35] Concerning the calculation of the ^{15}N chemical shifts, the typical error associated to the BLYP functional is much larger, that is, of the order of approximately 21 ppm for simple model compounds.[35] Recently, it has been shown for platinum(IV) and iridium(III) complexes, that using the PBE0 functional and taking onto account relativistic effects and spin–orbit coupling the agreement between measured and calculated chemical shifts of N atoms bound to transition metal atoms can be improved.[39] Using this approach the root mean square deviation of ^{15}N chemical shift with respect to the experimental values is approximately 8 ppm, whilst larger differences (13–16 ppm) are observed for N coordinated to a transition metal and having in *trans* position a Cl or S donor atom.[39] To make the comparison with experimental

data more stringent, the ^{15}N chemical shifts have been computed according to reference [39], namely using the PBE0 functional[58] (with 25% of exact exchange) and the triple-ξ singly polarized basis set TZP. Relativistic effects were taken into account with the zero-order regular approximation (ZORA), which includes spin–orbit effects.[59,60] The MM atoms were included as point charges. The calculations were carried out using the ADF code.[61–63] Since the method is more computational demanding than the one based on BLYP functional combined with norm conserving pseudo-potentials of the Martins–Troullier type, the calculations of chemical shifts were carried out by averaging over 30 equally spaced snapshots extracted from the last 10 ps of the QM/MM trajectories. For comparison purpose the ^{15}N chemical shifts have also been calculated by using the BLYP functional combined with pseudo-potentials of the Martins–Troullier type (Table S6 in the Supporting Information).

The chemical shielding constants were then converted to NMR chemical shifts relative to tetramethylsilane (TMS) in the case of ^{1}H and ^{13}C nuclei, and liquid ammonia in the case of ^{15}N nuclei. For the calculation of ^{13}C and ^{15}N chemical shifts we introduced secondary references, namely C_2H_6 for ^{13}C,[64] and $PtCl_2(NH_3)_2$ (cisplatin) in water for ^{15}N (see the Supporting Information for more details). The chemical shielding constant of cisplatin (the secondary reference) was obtained by an additional QM/MM simulation (see the Supporting Information) by using the same procedure as for the Pt-adduct.

The CD spectra were calculated with the web interface DichroCalc[65,66] by averaging 100 snapshots taken over the last 10 ps of the QM/MM trajectories of the apo protein and Pt-adduct in solution.

The same snapshots were used to carry out an analysis of the secondary structure content with DSSP.[32,33]

In addition, an analysis of the average dihedral angles ϕ, ψ, ω, and $\chi 1$ and of the hydrogen bonds formed in the apo protein and in the Pt-adduct, was performed using the web server VADAR.[34] The average values and their standard deviations were calculated over 15 snapshots along the QM/MM simulations (see Tables S8–S14 and Figures S3 and S4 in the Supporting Information).

Experimental Section

Solution NMR experiments

The ^{15}N-labeled complex, *cis*-$[PtCl_2(^{15}NH_3)_2]$, was dissolved immediately prior to use in pure deoxygenated water at 2 mM final concentration. The complex solution was extensively vortexed and sonicated and the exact Pt concentration was determined by atomic absorption spectroscopy using a Varian 880Z instrument.

NMR spectroscopy experiments were recorded on a fully ^{15}N-labeled and selectively ^{13}C-cysteine-labeled Atox1 (^{15}N,^{13}C-Cys Atox1 hereafter), purchased from Giotto Biotech S.r.l. (Sesto Fiorentino, Italy), in phosphate buffer (50 mM, pH 7.0) at 25 °C under inert N_2 atmosphere, in the absence of any reducing agent. ^{15}N-labeled cisplatin was added to the protein sample to obtain a 100 μM equimolar mixture and the reaction was monitored through ^{1}H,^{15}N and ^{1}H,^{13}C HSQC spectra, acquired using a gradient-enhanced sequence in which coherence selection and water suppression were achieved by gradient pulses. Sixteen transients were acquired over an F2 (^{1}H) spectral width of 14 ppm into 1024 complex data points for each of 256 t_1 increments with an F1 spectral width of 100 ppm centered at −50 ppm (for ^{15}N detection) or 70 ppm centered at 40 ppm (for ^{13}C), with a delay $1/(4J_{XH})$ of 2.78 ms (X = ^{15}N) or 1.72 ms (X = ^{13}C), and a recycle delay of 1.0 s. The spectra were collected on a Bruker Avance 600 UltraShield Plus magnet using a triple-resonance (TXI) probe equipped with pulsed-field gradients along the *z* axis, processed using the standard Bruker software (TOPSPIN).

Acknowledgements

V.C. acknowledges the Deutsche Forschungsgemeinschaft (DFG) for financial support (Grant No. CA 973/8-1). The authors thank the University of Bari and the Consorzio Interuniversitario di Ricerca in Chimica dei Metalli nei Sistemi Biologici (CIRCMSB), the Italian Ministero dell'Università e della Ricerca (PON 01078 and PRIN 2010M2JARJ), and the European Commission (COST Action CM1105) for support. The computing time granted by the John von Neumann Institute for Computing (NIC) and provided on the supercomputer JUROPA at Jülich Supercomputing Centre (JSC) is also gratefully acknowledged.

Keywords: cisplatin · computer chemistry · hybrid QM/MM simulations · NMR chemical shifts · molecular modeling

[1] M. A. Fuertes, C. Alonso, J. M. Perez, *Chem. Rev.* **2003**, *103*, 645 – 662.
[2] Y. Jung, S. J. Lippard, *Chem. Rev.* **2007**, *107*, 1387 – 1407.
[3] L. Kelland, *Nat. Rev. Cancer* **2007**, *7*, 573 – 584.
[4] M. D. Hall, M. Okabe, D. W. Shen, X. J. Liang, M. M. Gottesman, *Annu. Rev. Pharmacol. Toxicol.* **2008**, *48*, 495 – 535.
[5] B. Lippert, in *Cisplatin: Chemistry and Biochemistry of a Leading Anticancer Drug* (Ed.: B. Lippert), Helvetica Chimica Acta, Zürich, **2006**, pp. 377 – 403.
[6] D. Wang, S. J. Lippard, *Nat. Rev. Drug Discovery* **2005**, *4*, 307 – 320.
[7] V. Brabec, *Prog. Nucleic Acid Res. Mol. Biol.* **2002**, *71*, 1 – 68.
[8] E. R. Jamieson, S. J. Lippard, *Chem. Rev.* **1999**, *99*, 2467 – 2498.
[9] Z. H. Siddik, *Oncogene* **2003**, *22*, 7265 – 7279.
[10] S. B. Howell, R. Safaei, C. A. Larson, M. J. Sailor, *Mol. Pharmacol.* **2010**, *77*, 887 – 894.
[11] R. Safaei, *Cancer Lett.* **2006**, *234*, 34 – 39.
[12] R. Safaei, S. B. Howell, *Crit. Rev. Oncol. Hematol.* **2005**, *53*, 13 – 23.
[13] T. Furukawa, M. Komatsu, R. Ikeda, K. Tsujikawa, S. Akiyama, *Curr. Med. Chem.* **2008**, *15*, 3268 – 3278.
[14] M. T. Kuo, H. H. W. Chen, I.-S. Song, N. Savaraj, T. Ishikawa, in *Cancer and Metastasis Reviews, Vol. 26*, Kluwer – Plenum, **2007**, pp. 71 – 83.
[15] S. Ishida, J. Lee, D. J. Thiele, I. Herskowitz, *Proc. Natl. Acad. Sci. USA* **2002**, *99*, 14298 – 14302.
[16] M. Komatsu, T. Sumizawa, M. Mutoh, Z. S. Chen, K. Terada, T. Furukawa, X. L. Yang, H. Gao, N. Miura, T. Sugiyama, S. Akiyama, *Cancer Res.* **2000**, *60*, 1312 – 1316.
[17] G. Samimi, R. Safaei, K. Katano, A. K. Holzer, M. Rochdi, M. Tomioka, M. Goodman, S. B. Howell, *Clin. Cancer. Res.* **2004**, *10*, 4661 – 4669.
[18] N. V. Dolgova, S. Nokhrin, C. H. Yu, G. N. George, O. Y. Dmitriev, *Biochem. J.* **2013**, *454*, 147 – 156.
[19] M. E. Palm-Espling, C. D. Andersson, E. Bjorn, A. Linusson, P. Wittung-Stafshede, *PloS ONE* **2013**, *8*, e70473.
[20] R. Safaei, M. H. Maktabi, B. G. Blair, C. A. Larson, S. B. Howell, *J. Inorg. Biochem.* **2009**, *103*, 333 – 341.
[21] S. Itoh, H. W. Kim, O. Nakagawa, K. Ozumi, S. M. Lessner, H. Aoki, K. Akram, R. D. McKinney, M. Ushio-Fukai, T. Fukai, *J. Biol. Chem.* **2008**, *283*, 9157 – 9167.
[22] T. H. Nguyen, F. Arnesano, S. Scintilla, G. Rossetti, E. Ippoliti, P. Carloni, G. Natile, *J. Chem. Theor. Comp.* **2012**, *8*, 2912 – 2920.
[23] F. Tadini-Buoninsegni, G. Bartolommei, M. R. Moncelli, G. Inesi, A. Galliani, M. Sinisi, M. Losacco, G. Natile, F. Arnesano, *Angew. Chem.* **2014**, *126*, 1321 – 1325; *Angew. Chem. Int. Ed.* **2014**, *53*, 1297 – 1301.

[24] V. Calandrini, F. Arnesano, A. Galliani, T. H. Nguyen, E. Ippoliti, P. Carloni, G. Natile, *Dalton Trans.* **2014**, *43*, 12085 – 12094.
[25] F. Arnesano, L. Banci, I. Bertini, I. C. Felli, M. Losacco, G. Natile, *J. Am. Chem. Soc.* **2011**, *133*, 18361 – 18369.
[26] C. M. Sze, Z. Shi, G. N. Khairallah, L. Feketeova, R. A. O'Hair, Z. Xiao, P. S. Donnelly, A. G. Wedd, *Metallomics* **2013**, *5*, 946 – 954.
[27] X-ray studies show that the binding in the solid state is completely different. Indeed, in the 1:1 complex between human Atox1 and cisplatin (A. K. Boal, A. C. Rosenzweig, *J. Am. Chem. Soc.* **2009**, *131*, 14196 – 14197), the platinum ion loses all of its ligands and binds to N and S atoms of Cys12 and to S atom of Cys15 with the two sulfurs in *trans* positions, along with an external tris(2-carboxyethyl)phosphine (TCEP), a reducing agent used in the preparation of the sample for the crystallization process. In the same paper is also reported the X-ray structure of a 1:2 adduct in which two Atox1 molecules bind via Cys15 residues to platinum, which retains the two ammines of cisplatin.
[28] J. M. Wang, P. Cieplak, P. A. Kollman, *J. Comput. Chem.* **2000**, *21*, 1049 – 1074.
[29] V. Hornak, R. Abel, A. Okur, B. Strockbine, A. Roitberg, C. Simmerling, *Proteins Struct. Funct. Bioinf.* **2006**, *65*, 712 – 725.
[30] W. L. Jorgensen, J. Chandrasekhar, J. D. Madura, R. W. Impey, M. L. Klein, *J. Chem. Phys.* **1983**, *79*, 926 – 935.
[31] I. Anastassopoulou, L. Banci, I. Bertini, F. Cantini, E. Katsari, A. Rosato, *Biochemistry* **2004**, *43*, 13046 – 13053.
[32] R. P. Joosten, T. A. H. te Beek, E. Krieger, M. L. Hekkelman, R. W. W. Hooft, R. Schneider, C. Sander, G. Vriend, *Nucleic Acids Res.* **2011**, *39*, D411 – D419.
[33] W. Kabsch, C. Sander, *Biopolymers* **1983**, *22*, 2577 – 2637.
[34] L. Willard, A. Ranjan, H. Zhang, H. Monzavi, R. F. Boyko, B. D. Sykes, D. S. Wishart, *Nucleic Acids Res.* **2003**, *31*, 3316 – 3319.
[35] J. R. Cheeseman, G. W. Trucks, T. A. Keith, M. J. Frisch, *J. Chem. Phys.* **1996**, *104*, 5497 – 5509.
[36] CPMD, http://www.cpmd.org/; Copyright IBM Corp 1990 – 2008, Copyright MPI für Festkörperforschung Stuttgart 1997 – 2001.
[37] T. G. Appleton, J. W. Connor, J. R. Hall, P. D. Prenzler, *Inorg. Chem.* **1989**, *28*, 2030 – 2037.
[38] T. G. Appleton, J. R. Hall, S. F. Ralph, *Inorg. Chem.* **1985**, *24*, 4685 – 4693.
[39] J. Vicha, M. Patzschke, R. Marek, *Phys. Chem. Chem. Phys.* **2013**, *15*, 7740 – 7754.
[40] R. Car, M. Parrinello, *Phys. Rev. Lett.* **1985**, *55*, 2471 – 2474.
[41] P. Carloni, U. Rothlisberger, in *Theoretical Biochemistry: Processes and Properties of Biological Systems, Vol. 9* (Ed.: L. A. Eriksson), Elsevier, **2001**, pp. 215 – 251.
[42] M. Dal Peraro, P. Ruggerone, S. Raugei, F. L. Gervasio, P. Carloni, *Curr. Opin. Struct. Biol.* **2007**, *17*, 149 – 156.
[43] A. Laio, J. VandeVondele, U. Rothlisberger, *J. Phys. Chem. B* **2002**, *106*, 7300 – 7307.
[44] A. Laio, J. VandeVondele, U. Rothlisberger, *J. Chem. Phys.* **2002**, *116*, 6941 – 6947.
[45] C. Micheletti, F. Seno, A. Maritan, *Proteins Struct. Funct. Bioinf.* **2000**, *40*, 662 – 674.
[46] W. F. van Gunsteren, S. R. Billeter, A. A. Eising, P. H. Hünenberger, P. Krüger, A. E. Mark, W. R. P. Scott, I. G. Tironi, *Biomolecular Simulation: The GROMOS96 Manual and User Guide*, Vdf Hochschulverlag AG an der ETH Zürich, **1996**.
[47] A. D. Becke, *Phys. Rev. A* **1988**, *38*, 3098 – 3100.
[48] C. Lee, W. Yang, R. G. Parr, *Phys. Rev. B* **1988**, *37*, 785 – 789.
[49] N. Troullier, J. L. Martins, *Phys. Rev. B* **1991**, *43*, 1993 – 2006.
[50] O. A. von Lilienfeld, I. Tavernelli, U. Rothlisberger, D. Sebastiani, *J. Chem. Phys.* **2005**, *122*, 14113 – 14118.
[51] G. J. Martyna, M. E. Tuckerman, *J. Chem. Phys.* **1999**, *110*, 2810 – 2821.
[52] W. G. Hoover, *Phys. Rev. A* **1985**, *31*, 1695 – 1697.
[53] G. J. Martyna, M. L. Klein, M. Tuckerman, *J. Chem. Phys.* **1992**, *97*, 2635 – 2643.
[54] S. Nosé, *J. Chem. Phys.* **1984**, *81*, 511 – 519.
[55] A. Putrino, D. Sebastiani, M. Parrinello, *J. Chem. Phys.* **2000**, *113*, 7102 – 7109.
[56] D. Sebastiani, M. Parrinello, *J. Phys. Chem. A* **2001**, *105*, 1951 – 1958.
[57] T. Gregor, F. Mauri, R. Car, *J. Chem. Phys.* **1999**, *111*, 1815 – 1822.
[58] C. Adamo, V. Barone, *J. Chem. Phys.* **1999**, *110*, 6158 – 6169.
[59] E. van Lenthe, A. Ehlers, E.-J. Baerends, *J. Chem. Phys.* **1999**, *110*, 8943 – 8953.
[60] E. van Lenthe, J. G. Snijders, E. J. Baerends, *J. Chem. Phys.* **1996**, *105*, 6505 – 6516.
[61] ADF 2013, in *Scientific Computing and Modelling NV*, Vrije Universiteit, 1081 HV Amsterdam.
[62] C. Fonseca Guerra, J. G. Snijders, G. te Velde, E. J. Baerends, *Theor. Chem. Acc.* **1998**, *99*, 391 – 403.
[63] G. te Velde, F. M. Bickelhaupt, E. J. Baerends, C. Fonseca Guerra, S. J. A. van Gisbergen, J. G. Snijders, T. Ziegler, *J. Comput. Chem.* **2001**, *22*, 931 – 967.
[64] U. F. Röhrig, D. Sebastiani, *J. Phys. Chem. B* **2008**, *112*, 1267 – 1274.
[65] N. A. Besley, J. D. Hirst, *J. Am. Chem. Soc.* **1999**, *121*, 9636 – 9644.
[66] B. M. Bulheller, J. D. Hirst, *Bioinformatics* **2009**, *25*, 539 – 540.

Received: March 29, 2014
Published online on August 8, 2014